frontiers | Frontiers in Earth Science

TYPE Original Research
PUBLISHED 16 January 2023
DOI 10.3389/feart.2022.1043770

OPEN ACCESS

EDITED BY
Xingqi Liu,
Capital Normal University, China

REVIEWED BY
Kunshan Bao,
South China Normal University, China
Enfeng Liu,
Shandong Normal University, China

*CORRESPONDENCE
Yongming Han,
yongming@ieecas.cn

SPECIALTY SECTION
This article was submitted to Quaternary Science, Geomorphology and Paleoenvironment,
a section of the journal
Frontiers in Earth Science

RECEIVED 14 September 2022
ACCEPTED 31 October 2022
PUBLISHED 16 January 2023

CITATION
Jiang H, Han Y, Tang Y, Fan H, Liu B and Arimoto R (2023), Elemental data for Gonghai Lake sediments show significant effects of human activities on weathering processes after 1550 CE.
Front. Earth Sci. 10:1043770.
doi: 10.3389/feart.2022.1043770

Elemental data for Gonghai Lake sediments show significant effects of human activities on weathering processes after 1550 CE

Hong Jiang[1,2,3], Yongming Han[1,2,4,5]*, Yalan Tang[1,2,3], Huimin Fan[1], Bo Liu[6] and Richard Arimoto[1]

[1]State Key Laboratory of Loess and Quaternary Geology, Institute of Earth Environment, Chinese Academy of Sciences, Xi'an, China, [2]School of Human Settlements and Civil Engineering, Xi'an Jiaotong University, Xi'an, China, [3]University of Chinese Academy of Sciences, Beijing, China, [4]Center for Excellence in Quaternary Science and Global Change, Chinese Academy of Sciences, Xi'an, China, [5]National Observation and Research Station of Regional Ecological Environment Change and Comprehensive Management in the Guanzhong Plain, Xi'an, China, [6]Xi'an Institute for Innovative Earth Environment Research, Xi'an, China

The international Anthropocene Working Group has recognized the mid-20th centrury (ca. 1950 CE) as the onset of the Anthropocene, but human activities in China altered the land cover and influenced weathering processes much earlier. Changes in the elemental composition of sediment since 1000 CE from Gonghai Lake were studied, using X-ray Fluorescence element scanning (average time-resolution 3 years), to investigate the human impacts on weathering over time. We found that aluminum (Al) and calcium (Ca) containing minerals vary in the resistance to chemical weathering, and the concentrations of Al and Ca provide insights into the intensities of mechanical and chemical weathering respectively. The correlations between Al and Ca concentrations in these two periods, 1000–1550 CE and 1550–1950 CE changed from negative to positive, owing to that agricultural activities evidently enhanced both mechanical and chemical weathering during the latter stage. In addition, the Al and Ca concentrations recorded a border reclamation project in the 16th century and two catastrophic population decreases from 1630s to 1640s and 1850s–1870s. After 1950 CE, the concentrations of Al and Ca became uncorrelated, because weathering processes around Gonghai Lake were impacted by the enhanced anthropogenic perturbations in the Anthropocene.

KEYWORDS

anthropocene, human activities, weathering, major elements, sediment, North China

1 Introduction

In recent decades, human activities have profoundly affected the Earth system, making conditions that are markedly different from those in the Holocene. Therefore, the concept of "Anthropocene" has been proposed (Crutzen, 2002; Lewis and Maslin, 2015; Waters et al., 2016). At present, the international Anthropocene Working Group (AWG) has designated the mid-20th century (i.e., ca. 1950 CE, "CE" is the abbreviation for Common Era) as the onset of the Anthropocene (Waters et al., 2018). Moreover, numerous geological records have shown that human perturbations of the environment in China significantly increased after 1950 CE (Han et al., 2011; Han et al., 2016; Liu et al., 2020; Liu et al., 2021).

Nonetheless, there were substantive effects of human activities in China during historical times. For example, agricultural activities caused a large scale of deforestation to reclaim farmlands in monsoonal areas of China, and this not only influenced the regional carbon cycle (Ge et al., 2008), but also accelerated the weathering of soils (Zong et al., 2010; Wu et al., 2015; Chen et al., 2020). In addition, these changes in weathering processes caused frequent flooding and rechanneling of the Yellow River (Tan, 1962), and accelerated the degradation of lakes in the middle and lower reaches of the Yangtze River (Huang, 2001). However, the understanding of human activities evolution over historical times from geological records in the densely populated China is still limited.

The history of human activities is very short in comparison with geological history of the earth, and thus understanding this history of human activities requires high-resolution archives. Many lakes have relatively high sedimentation rates, and when combined with continuous chronological records, the sedimentary data can be used for high-resolution reconstructions. Aluminum (Al), calcium (Ca), silicon (Si), iron (Fe), and potassium (K) are major elements in the Earth's crust, and they account for a large portion of the mass in lake sediments. Among them, Al, Si, Fe, and K are cardinal elements of silicate minerals, which are not apt to chemical weathering, whereas Ca mainly exists in carbonate, which are apt to chemical weathering (Shen et al., 2010). The concentrations of these elements in lake sediments have been shown to reflect changes in the weathering of soils around lakes owing to their various geochemical behaviors (Shen et al., 2010; Liu et al., 2014). We reconstructed the weathering history since 1000 CE through the determination of Al, Ca, Si, K, Fe, and Ti concentrations and rubidium to strontium (Rb/Sr) ratios from sediments of the sub-alpine Gonghai Lake in North China. Among them, Ti is a known refractory element indicating mechanical weathering, the Rb/Sr ratio is a widely used proxy for chemical weathering, and in general, higher Ti concentrations indicate stronger mechanical weathering, whereas lower Rb/Sr ratios indicate stronger chemical weathering (Shen et al., 2010). The high-resolution historical sequences of the above proxies for Gonghai Lake sediments can provide meaningful insights into the weathering evolution in North China influenced by intensive agricultural activities before modern times, and contribute to the understanding of the historical background of the Anthropocene starting at *ca.* 1950 CE that was proposed by the AWG.

2 Study area

Gonghai Lake (38°54′N, 112°14′E, 1860 m a.s.l., area of 0.36 km^2) is located in Ningwu County, Shanxi Province, North China (Figure 1A) and is in the eastern part of the Chinese Loess Plateau. It is a sub-alpine lake with a small basin size (1.0 km^2) and limited runoff injection, and its image is shown in Figure 1C.

The bedrock in the small catchment is dominated by sandstone, the regional soil in its surrounding areas mainly consists of mountain-meadow soil, meadow soil, cinnamon soil, brown soil and chestnut soil, of which cinnamon soil is the major type (Liu et al., 2011). There are three kinds of landforms around the small catchment: basins, loess hills and mountains. The elevation of the basin areas is relatively low, most of them are reclaimed as farmland or have been developed into settlements. The vegetation of loess hilly area is disturbed by human activities, with serious land desertification, and its forest coverage is about 10%. The mountain areas have relatively good vegetation coverage, dominated by deciduous and coniferous forests.

Ningwu County has an annual precipitation of 445 mm, 77% of which occurs from June to September (China Meteorological Data Service Centre, http://data.cma.cn). The prevailing wind is from the south and east in summer, and from the north and west in winter, with a typical monsoon climate.

3 Sample collection

In November 2019, cores were collected with a gravity corer at the central deep water position (~9.5 m, Figure 1B) in Gonghai Lake. A prior study (Liu et al., 2014) showed that the age of Gonghai Lake sediments at depth of ~2.0 m was ~1.0 ka. There are three physical truths as follows: 1) the limited length of the gravity corer (2 m); 2) the need to ensure top of the core was undisturbed; 3) while trying to fully fill the core tube, the top of the core was apt to be disturbed owing to striking and the sequential shocking. To address the above three cases, the shorter cores (1.0–1.5 m) were collected initially, then tried to fully fill the core tube to obtain the longer cores (1.8–2.0 m). The length of the obtained shorter and longer cores are shown in Table 1. Thereafter, we have to connect one shorter core and one longer core to meet the desire length and chronological span. The shorter core GH19C and longer core GH19J were connected by depth-series plots of Rb/Sr according to the law of superposition (Shu, 2010, Figure 2) as following.

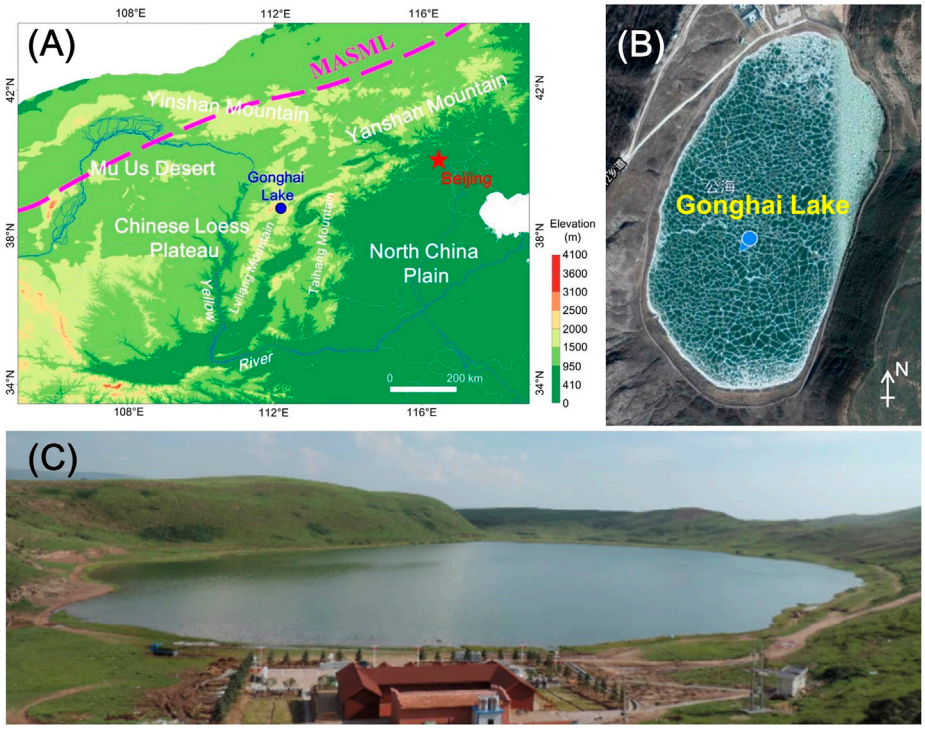

FIGURE 1
The study area: **(A)** location of Gonghai Lake; **(B)** core sampling site; and **(C)** image of Gonghai Lake (Chen et al., 2017). The magenta dashed line is the modern Asian summer monsoon limit (MASML, after Liu et al., 2014).

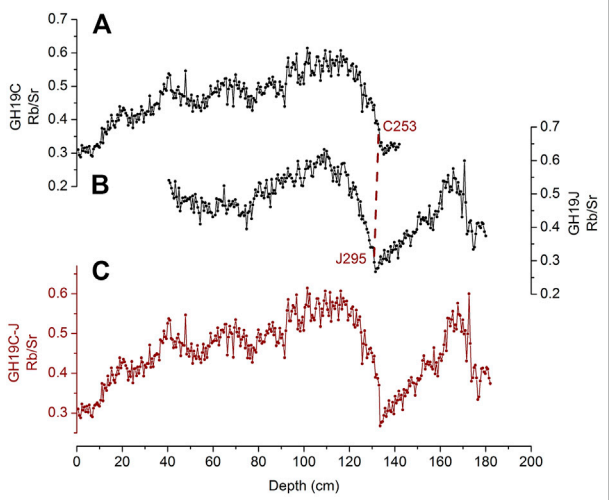

FIGURE 2
Connection of cores **(A)** GH19C and **(B)** GH19J by a matching of the significant decreases in Rb/Sr ratios versus depth; this was the method used to produce **(C)** the connected GH19C-J data. The reason why Rb/Sr of the top of GH19J were not measured was introduced in Section 3.

Sample C253 and J295 are the last point of abrupt decrease in Rb/Sr ratios at depths between 120 and 140 cm in the two cores (Figure 2), which indicate an abrupt change in chemical weathering (In this study, the samples were named according to the alphabetical letter of the cores and the number of the samples from top to bottom in the core. For example, the sample from core GH19B that numbered 130 was named B130.) This is also supported by the abrupt increases in Ca concentrations and decreases in Fe and Ti concentrations in the corresponding layer (Figures 5A–C). As such, GH19C and GH19J were connected at points of samples C253 and J295. The connected core was renamed as GH19C-J and dated.

Owing to the disturbance on the top of the longer cores while sampling, the proxies of samples from them were not measured (Figure 2B, Figures 5A,D).

4 Methods

4.1 Dating data acquirements

For chronological control points above ~40 cm of the cores, they were dated *via* ^{137}Cs and ^{210}Pb measurements of freeze-dried

TABLE 1 The actual length of the shorter and longer cores.

Code	Shorter cores			Longer cores		
	GH19B	GH19C	GH19D	GH19A	GH19J	GH19K
Length (m)	1.35	1.42	1.03	1.8	1.8	2.0

TABLE 2 AMS^{14}C dating of plant residues (the calendar year correction mode is Intcal20).

Sample codes	Laboratory codes	^{14}C a BP	Error (2σ)	cal Year (CE)	cal error range (CE)
B130	XA52456	260	30	1648	1636–1663
K133	XA52681	270	30	1643	1633–1661
B205	XA52680	430	30	1450	1438–1470
A300	XA52668	815	30	1241	1219–1264
A301	XA52669	655	30	1365	1359–1389
J371	XA52670	990	30	1034	1020–1048

samples. The ^{137}Cs and ^{210}Pb measurements were conducted in Key Laboratory of Tibetan Environment Changes and Land Surface Processes, Chinese Academy of Sciences, Beijing, China.

For chronological control points below ~60 cm, they were dated *via* accelerator mass spectrometry ^{14}C (AMS ^{14}C) measurements of plant residues. The AMS ^{14}C analyses were conducted in the Institutional Center for Shared Technologies and Facilities of the Institute of Earth Environment, Chinese Academy of Sciences, Xi'an, China. The AMS ^{14}C dating data was corrected by the IntCal20 model (calib.org/calib/calib.html). Due to low quantities of plant residues in the cores, only six plant residues sufficient for AMS ^{14}C dating were obtained from the six shorter/longer cores, the dating data of them are listed in Table 2.

For chronological control points between ~40 and ~60 cm, they were dated *via* a novel method that making use of data from both ^{210}Pb and AMS ^{14}C measurements. The details are provided in Section 5.2.2.

The connected core GH19C-J was dated based on the above chronological control points through peak/valley correspondence of the depth-series plots of the proxies, according to the law of superposition (Shu, 2010). For samples of non-chronological control points, their ages were obtained by linear interpolations.

The details of the above dating processes are provided in the Section 5 Chronology.

4.2 Element concentration measurements

X-ray Fluorescence (XRF) scanning was employed for the element concentration measurements. It uses X-rays from an excitation source (X-ray tube) to irradiate the samples, and that causes secondary fluorescent emissions, which are detected and quantified. In this way, the concentrations of selected elements (indicated by their peculiar ray counts per second (cps)) can be quantified. The major advantages of XRF are that the method is rapid and non-destructive (Davies et al., 2015).

For our analyses, the freeze-dried samples were ground and passed through a 100 mesh sieve and then made into 3.0 × 3.0 cm flakes. The XRF analyses were conducted in the Institutional Center for Shared Technologies and Facilities of the Institute of Earth Environment, Chinese Academy of Sciences, Xi'an, China (The instrument type is 4th Generation XRF Core Scanner, Avaatech). A total of 1416 samples from six shorter/longer cores were analyzed using these procedures. The results of measurements of 53 replicate samples show that the reproducibilities of Al, Si, Fe, Ca, K, Ti, Rb, and Sr are good. The average retest errors of Al, Si, Rb, Sr range from 5 to 8%, whereas those of Fe, K, Ca, Ti are within 5%.

4.3 Total organic carbon content measurements

In sediments, carbon mainly exists in carbonate and organic matters. To measure total organic carbon (TOC) contents, the carbonate must be removed beforehand. In this study, the carbonate was removed by incubating aliquots of the samples that passed through the 100 mesh sieve in 2 mol L^{-1} hydrochloric acid for 24 h. The samples were

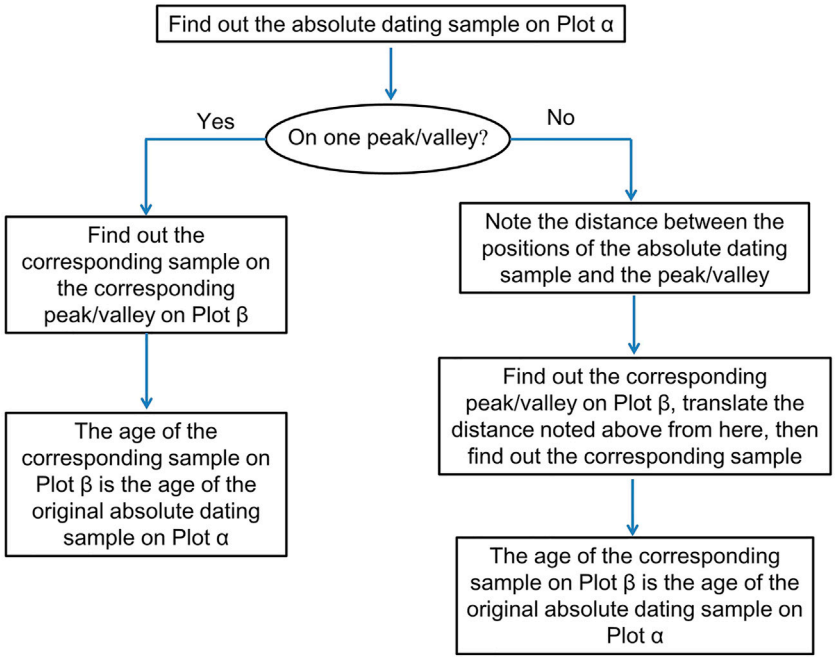

FIGURE 3
Steps in the relative dating by the proxy-depth plots for multiple cores. The proxy-depth plot with the absolute dating samples is designated as Plot α, and the plot of the same proxies of the core to be dated is designated as Plot β.

stirred three times during this step. After drying, the decarbonated samples were ground and passed through a 200 mesh sieve; 25–40 mg of the samples was wrapped in tin boats. Afterwards, TOC contents were measured by a Vario El III element analyzer (Elementar, Germany), in Key Lab of Aerosol Chemistry & Physics of the Institute of Earth Environment, Chinese Academy of Sciences, Xi'an, China. A replicate sample was measured every 11 samples to ensure data quality. The average retest error is 0.9%.

5 Chronology

5.1 General dating methods

Samples for ^{210}Pb and ^{137}Cs dating were taken from core GH19D, and samples for AMS ^{14}C dating were taken from cores GH19 A/B/J/K. The method for finding out the corresponding samples of the absolute dating samples in the connected core GH19C-J is shown in Figure 3. Plots of Ca, Fe, Ti concentrations and Rb/Sr ratios versus depth were used for determining the relative positions of the corresponding samples in GH19C-J. The correspondences of the samples and dating procedures are shown in Figure 4C and Figure 5.

5.2 Dating processes and results

5.2.1 Dating of samples above the 1952 CE ^{137}Cs marker

^{137}Cs and ^{210}Pb$_{ex}$ are only suitable for dating of relatively young sediments deposited in the last 200 years. Therefore, the dating of GH19C-J described in this sub-section was only conducted on the upper part from the shorter core GH19C.

Based on the ^{137}Cs activity plot (Figure 4A), the earliest high value in ^{137}Cs activity is at depth of 19.4 cm (sample D035), which is the 1963 CE ^{137}Cs marker; the initially detectable in ^{137}Cs activity is at depth of 26.0 cm (D047), which is the 1952 CE ^{137}Cs marker (Wan et al., 2016). The age of the uppermost sample (D001) is the sampling year (2019 CE).

A common problem with ^{210}Pb CRS model dating is that the interval dated as 1963 CE often deviates from the 1963 CE ^{137}Cs marker. As such, Liu et al. (2009) proposed a method for ^{210}Pb dating in combination with the 1963 CE ^{137}Cs marker, whereby a core is divided into upper and lower sections above and below this marker respectively, which are then each dated by the ^{210}Pb CRS model.

For the core above the depth of the 1963 CE ^{137}Cs marker, the following equation can be obtained:

$$\frac{1-e^{-\lambda(T_0-1963)}}{A_0-A_w}=\frac{1-e^{-\lambda(T_0-T_m)}}{A_0-A_m} \quad (1)$$

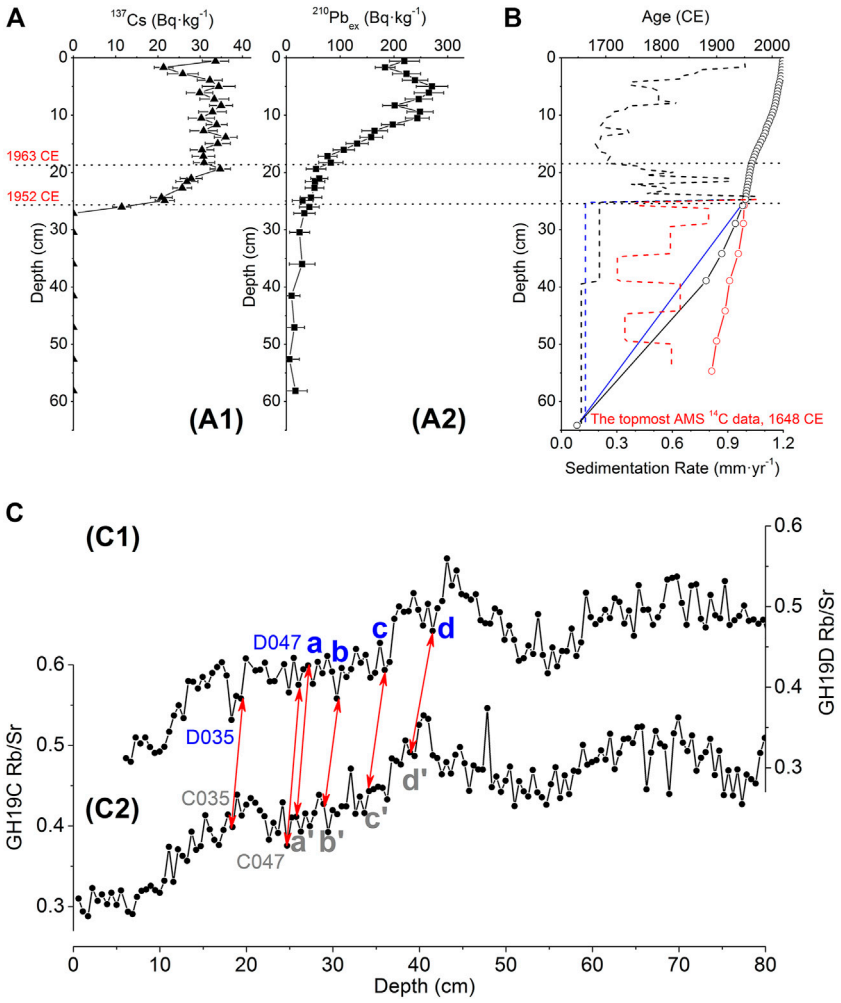

FIGURE 4
(A) Changes in **(A1)** ^{137}Cs and **(A2)** ^{210}Pb$_{ex}$ activities versus depth in core GH19D. Red text indicates the 1963 and 1952 CE ^{137}Cs marker. The grey error bars indicate standard deviation (s. d.). **(B)** Age-depth plots of GH19C-J obtained by Method I (red), II (blue) and III (black), the small circles are chronological control points. The dashed lines of different colors are plots of sedimentation rate versus depth obtained by the corresponding age-depth plots of the same color. **(C)** Rb/Sr ratios versus depth for cores **(C1)** GH19D and **(C2)** GH19C and their chronological correspondence. The blue text indicates samples with absolute dating data, the grey text indicates samples with relative dating data, and red double arrows indicate the correspondence between the dating points. The a–a′, b–b′, c–c′, d–d′ (the numbers of these samples are D049–C049, D055–C055, D065–C065, D075–C074, respectively) are the correspondence of age data obtained by Method III.

where T_m is the undetermined age of layer m, T_0 is the sampling year (2019 CE, in this study), λ is the decay constant of ^{210}Pb (0.0311 years^{-1}), A_0, A_m, and A_w are the cumulative amounts of ^{210}Pb$_{ex}$ per unit area of the whole core, below the depth of the undetermined age, and below the 1963 CE ^{137}Cs marker (in Bq·cm^{-2}), respectively.

The undetermined age T_m can then be calculated as:

$$T_m = T_0 + \frac{1}{\lambda}\ln\left\{1 - \left[1 - e^{-\lambda(T_0-1963)}\right]\frac{A_0 - A_m}{A_0 - A_w}\right\} \quad (2)$$

For samples below the 1963 CE ^{137}Cs marker, based on the CRS model, the ratio of A_m to A_w is:

$$\frac{A_m}{A_w} = e^{-\lambda(1963-T_m)} \quad (3)$$

The undetermined age T_m can then be calculated as:

$$T_m = 1963 - \frac{1}{\lambda}\ln\left(\frac{A_w}{A_m}\right) \quad (4)$$

Eq. 4 yielded an age for sample D047 of 1951 CE, which is consistent with the 1952 CE age from the onset of ^{137}Cs activity (Figure 4A). This agreement indicates that all the ages between 1952 and 1963 CE calculated with Eq. 4 are reliable. The ages of all samples above sample D035 with ^{210}Pb$_{ex}$ data were calculated

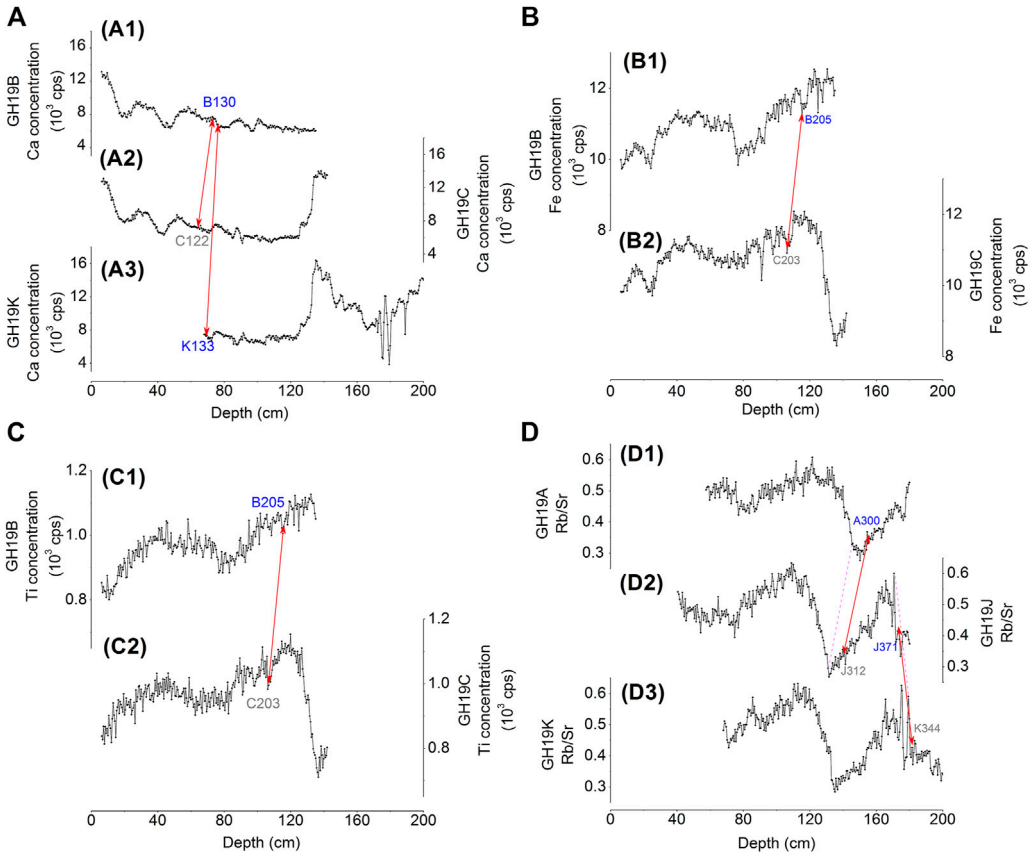

FIGURE 5
(A) Ca concentration-depth plots for cores **(A1)** GH19B, **(A2)** GH19C, **(A3)** GH19K; **(B)** Fe concentration-depth plots of **(B1)** GH19B, **(B2)** GH19C; **(C)** Ti concentration-depth plots of **(C1)** GH19B, **(C2)** GH19C; **(D)** Rb/Sr-depth plots of **(D1)** GH19A, **(D2)** GH19J, **(D3)** GH19K, and their chronological correspondence. The blue text indicates samples with absolute dating data, the grey text indicates samples with relative dating data, and red double arrows indicate the correspondence between the dating points; the magenta dashed line indicates the corresponding inflection point of the sign. The reason why the proxies of the top of GH19 A/J/K were not measured was introduced in Section 3.

with Eq. 2. The ages of samples without $^{210}Pb_{ex}$ data were linearly interpolated based on the nearest dating data obtained from $^{210}Pb_{ex}$ above and below such samples.

According to the method in Figure 3, the corresponding samples in GH19C of samples with dating data in GH19D were found out, based on Rb/Sr ratios versus depth plots (Figure 4C). Samples above the depth of C047 and D047 are corresponding to each other.

5.2.2 Dating samples below the 1952 CE ^{137}Cs marker

A previous study showed that it was not reliable to date samples below the 1952 CE ^{137}Cs marker *via* the CRS model (Wan et al., 2016). Therefore, we used two other methods based on: (method I) Eq. 4; (method II) linear interpolation between the 1952 CE ^{137}Cs marker and the uppermost AMS ^{14}C age. The two results are shown as red and blue lines in Figure 4B respectively. There is a significant difference between the two results. Therefore, we used a third method as following.

The $^{210}Pb_{ex}$ values do not decrease significantly below sample D075 (Figure 4A), and thus the ^{210}Pb dating for samples below sample D075 are unreliable. As such, we calculated the ^{210}Pb ages for samples above D075 (including D049, D055, D065, D075) using Eq. 4 (i.e., method I), and found out the corresponding samples of the four samples in core GH19C (including C049, C055, C065, C074, Figure 4C). On the other hand, the ages of the four samples were obtained with method II. We then calculated the averages of the two ages obtained *via* method I and II for the above four corresponding pairs of samples. This is the third method (method III). The age-depth plot obtained by method III is the black line in Figure 4B.

5.2.3 ^{14}C dating

Based on the method shown in Figure 3, we found out the corresponding samples in GH19C-J of the AMS ^{14}C dating

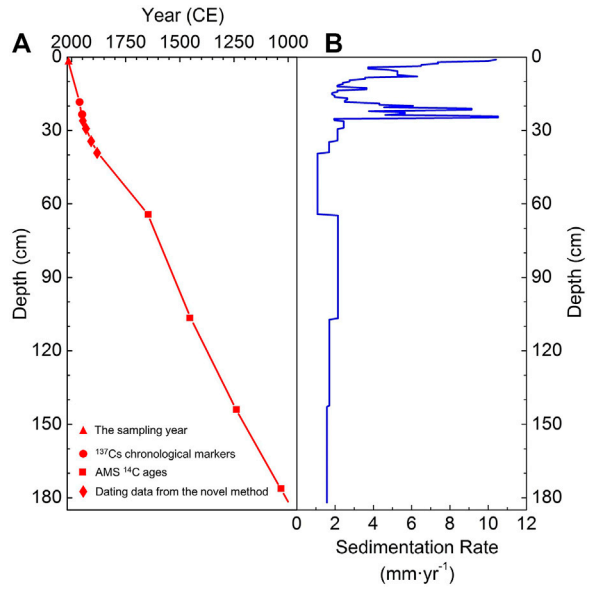

FIGURE 6
(A) Age-depth and **(B)** sedimentation rate-depth plots of the connected GH19C-J core.

samples in core GH19A/B/J/K. The details are shown in Figure 5. Sample J371 has AMS ^{14}C data and is a chronological control point, its calibrated age is 1034 CE. The basal depth of core GH19C-J is 182.0 cm. The sedimentation rate below sample J371 was assumed to be the same as that between the depths of the lowest two corresponding samples in GH19C-J, i.e., J312 and J371. This leads to a basal age for core GH19C-J of 988 CE.

Sample K133 was also AMS ^{14}C dated. Based on the method shown in Figure 3, this sample is corresponded with core GH19B at a level that is ~2 cm below sample B130 (Figure 5A), which is consistent with its age being 5 years older than sample B130.

5.2.4 Dating results

The dating results are shown in Figure 6. It is obtained that the time span for the connected core GH19C-J is ~1000 years (actually from 988 to 2019 CE). The connected core was divided at intervals of 0.5 cm, and 342 samples were obtained, so the average resolution is ~3 years. The sharpest change in Al, Ca concentrations and Rb/Sr ratios were linearly interpolated in the 1340s, which is near to the end of Medieval Warm Period (MWP, a time span of *ca.* 900–1300 CE; Wang, 2011). The age-depth plot is in agreement with the previous studies (Liu et al., 2014; Wan et al., 2016). The corresponding sedimentation rate-depth plot is shown in Figure 6B, and it shows relatively higher sedimentation rate during modern times.

6 Results and discussion

6.1 The source of the major elements of Gonghai Lake sediments

Due to the small size of the Gonghai Lake basin (1.0 km^2), the sediment materials form the catchment is limited, and thus a relatively large fraction of the sediments comes from atmospheric dust deposition. Moreover, the atmospheric dust can also be deposited in the small catchment, when the materials in the catchment are transported into the lake (*via* scouring or gravitational processes), the coarser particles are apt to be deposited near the lakeshore, whereas the finer particles, which is more likely from the atmospheric deposition, are apt to be transported in to the central part and be deposited (Chen et al., 2017). Moreover, the region around Gonghai Lake has a typical monsoon climate, the prevailing wind directions change with the seasons, so atmospheric dust from different directions can be deposited in the Gonghai Lake basin. From the above, it can be inferred that the obtained sediment core in the central part of Gonghai Lake can record environmental changes that have occurred in a relatively broad surrounding area.

6.2 Indicator selection for chemical and mechanical weathering

The concentration-depth plots of five major elements, including Si, Al, Fe, K, and Ca, are compared and contrasted in Figure 7. Among them, Si, Al, Fe and K mainly exist in silicate minerals, which account for most of the mass of the sediments (Shen et al., 2010). Trends of their concentration-depth plots are generally similar, and they are also similar to the plot for Ti, an element known to be refractory to chemical weathering (Figure 7E, Shen et al., 2010; Cheng et al., 2020). These are also supported by their Pearson's coefficients and significance levels (Figures 8A–D). In contrast, Ca mainly exists in carbonate minerals, which account for 3.9–9.4% (the average is 5.4%, relatively higher in the Medieval Warm Period and Current Warm Period, lower in the Little Ice Age) of the sediment over the last ca. 1000 years (Chen et al., 2018). The plot of Ca is negatively correlated with those of the above five elements (Figures 7A–F; Figure 8E). The correlation between Ca and Si, Al, Fe, K is consistent with a principal component analyses result in Gonghai Lake from a previous study (Liu et al., 2014).

Calcium carbonate ($CaCO_3$) is abundant on the Chinese Loess Plateau where Gonghai Lake is located, and is apt to chemical weathering, which is promoted by high humidity, temperature, and atmospheric CO_2 (Schlesinger and Durham, 2016). The weathering reaction is as follows.

$$CaCO_3 + CO_2 + H_2O \rightarrow Ca^{2+} + 2HCO_3^-$$

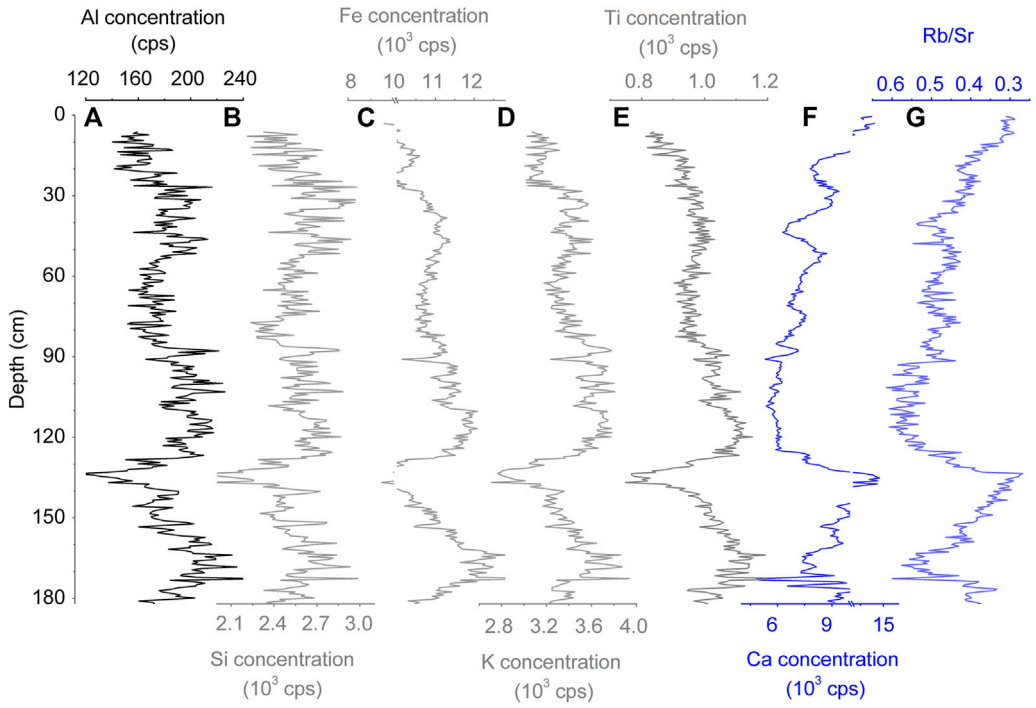

FIGURE 7
Concentration-depth plots of the elements of core GH19C-J: **(A–F)** Al, Si, Fe, K, Ti and Ca concentrations; **(G)** Rb/Sr ratios.

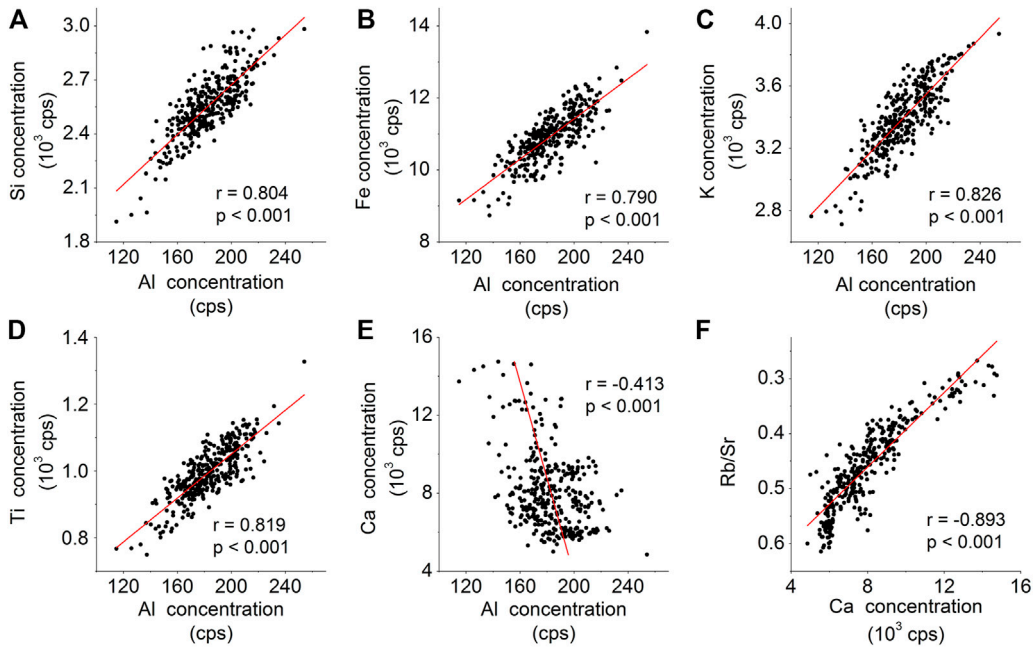

FIGURE 8
The Pearson correlation coefficient r and significance level *p*-value between Al concentrations and **(A)** Si, **(B)** Fe, **(C)** K, **(D)** Ti, **(E)** Ca concentrations, and **(F)** Ca concentration and Rb/Sr ratios. Age span of the above covers the last 1000 years.

After this process, Ca initially exists as Ca^{2+} ions in the aqueous phase. Under the semiarid climate, after a high rate of water evaporation, Ca is concentrated in fine particles in surface soils, which are easily transported by wind and can be deposited in Gonghai Lake. As such, Ca in lake sediments is strongly affected by chemical weathering.

The Ca in the Gonghai Lake sediment may also come from the Ca dissolved in the lake water. When the nutrient level of the lake water is higher, the production in the water will consume more CO_2 or HCO_3^- and thus raise the lake water pH, which is more favorable to the precipitation of Ca (Shen et al., 2010). In addition, the lake water evaporates faster when the climate is dry and/or hot, which is also conducive to the precipitation of Ca (Davies et al., 2015). The major exposed bedrock in the lake basin is sandstone (Liu et al., 2014) that contains less Ca than the surface soils of the Chinese Loess Plateau, in consideration of the small size of the Gonghai Lake basin, it can be deduced that a large portion of the Ca dissolved in the lake water comes from the Ca containing particles transported by wind as mentioned in the last paragraph.

In addition, Rb/Sr ratios, one typical indicator of chemical weathering in sedimentary records, are well negatively correlated with Ca concentrations (Figures 7F,G and Figure 8F). Moreover, the correlation between Ca and Ti concentrations is significantly negative (Figures 7E,F), indicating that Ca concentrations were hardly impacted by mechanical weathering. Therefore, it can be inferred that the Ca concentration of Gonghai Lake sediments is strongly affected by chemical weathering and can be an indicator of it. On the other hand, Al is one of the major elements that are resistant to chemical weathering and has fewer geological forms (Shen et al., 2010). Hence, Al concentration is selected as an indicator of mechanical weathering.

6.3 Overall changes in Al and Ca concentrations since 1000 CE

To evaluate the human activities on weathering, the conditions of climate change must be fully taken into consideration. Climatic conditions in China after 1000 CE can be separated into three stages as follows: 1) Medieval Warm Period (MWP, 900–1300 CE, the period of 1000–1300 CE belongs to this stage), 2) Little Ice Age (LIA, 1300–1900 CE), and 3) Current Warm Period (CWP, after 1900 CE) (Wang, 2011). The Al and Ca concentrations time-series plots show different trends during these three stages (Figures 9C,D) as follows. There is a large valley in the Al concentrations plot during the MWP, but a large peak in Ca concentrations plot is seen during the same period. In the first part of the LIA (1300–1550 CE, hereinafter referred to as LIA-1), Al concentrations were relatively high but Ca concentrations were relatively low. In the second part of the LIA (1550–1900 CE, LIA-2), Al concentrations were significantly lower than those in LIA-1, and roughly equivalent to those in the MWP. In contrast, Ca concentrations were generally higher in LIA-2 than those in LIA-1. During the CWP, Al and Ca concentrations varied in different ways over decadal scale, which may not be dominated by climate change. These are discussed below.

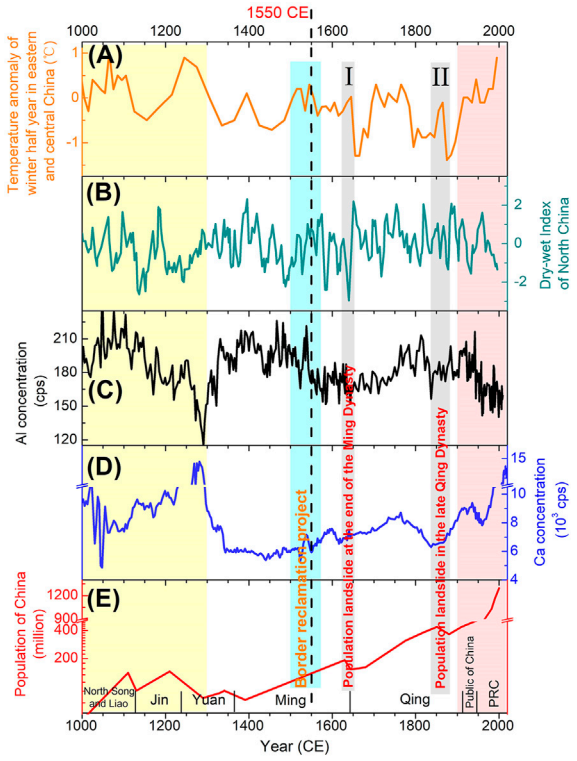

FIGURE 9
(A) Temperature anomaly for the winter half year in eastern and central China (Ge et al., 2003b), **(B)** dry-wet Index in North China (Zheng et al., 2006), **(C,D)** Al and Ca concentrations, and **(E)** population (Cao and Ge, 2005) since 1000 CE. In the past 1000 years, there were no significant changes in China's regional population proportion, so the historical sequence of population of the whole China can indicate the changes in intensity of human activities around Gonghai Lake. The yellow shadow indicates the Medieval Warming Period (MWP), the pink shadow indicates the Current Warming Period (CWP), the dash-dotted line is the boundary between Little Ice Age-1 (LIA-1) and Little Ice Age-2 (LIA-2), the cyan column indicates the border reclamation project period, and the 2 gray columns indicate the periods of population crashes. PRC is the abbreviation for People's Republic of China.

6.4 Changes in Al and Ca concentrations during the Medieval Warm Period and Little Ice Age-1 (1000–1550 CE)

LIA-1 was significantly colder than the MWP (Figure 9A, Wang, 2011), but was not wetter than the MWP (Figure 9B;

Wang et al., 2005; Zhang et al., 2008). Therefore, it was expected that less chemical weathering took place during LIA-1, thus Ca concentrations decreased from the MWP to LIA-1 (Figure 9D). Moreover, there was generally less vegetation during LIA-1 (Chen et al., 2015), thus more soils were exposed, leading to greater mechanical weathering and more Al erosion, so Al increased from the MWP to LIA-1 (Figure 9C).

This difference between the Al and Ca concentrations in Gonghai Lake sediments for the MWP versus LIA-1 is contrary to that in the loess-paleosol layers of the Chinese Loess Plateau, where the layers of loess (paleosol) correspond with the dry (wet) and cold (warm) periods (Chen et al., 1997). It shows that paleosol is relatively rich in Al and poor in Ca compared with loess (Chen et al., 1997). An important distinction between loess-paleosol and lake sediments is that loess-paleosol sediments are matrices of weathered materials, whereas lake sediments are repositories of weathered materials. If a particular type of substance is weathered, its concentration in the matrices will decrease, while that in the repositories will increase accordingly. This difference in the types of sedimentary environments can explain why the correlations between Al/Ca concentrations and climate change (one dominating factor of weathering) in lake sediments are opposite to those in the loess-paleosol sediments (Shen et al., 2010). Therefore, the contradiction mentioned in the first sentence of this paragraph indicates that changes in Al and Ca concentrations in Gonghai Lake sediments generally corresponded to climate change from the MWP to LIA-1 (1000–1550 CE), and thus the impacts of human activities were relatively weak during this period.

6.5 Changes in Al and Ca concentrations indicating intensified agricultural activities during LIA-2 (1550–1900 CE)

During LIA-2, the concentrations of Al and Ca were positively correlated, and the concentrations of both the elements increased with time (Figures 9C,D). This is unlike the patterns in the MWP and LIA-1 when they were negatively correlated, which cannot be solely explained by climate change, but may be related to human activities.

The changes in Al and Ca concentrations during LIA-2 were compared with the changes in population and high-resolution records of climate change (Figure 9). In the past 1000 years, there were no significant changes in China's regional population proportion, so the historical sequence of population of the whole China can indicate the changes in intensity of human activities around Gonghai Lake. The temperature anomaly of the winter half year in eastern and central China time-series plot was adopted as a measure of temperature change (Figure 9A; Ge et al., 2003b), and the dry-wet index in the North China time-series plot was adopt as a reflection of wetness change (Figure 9B; Zheng et al., 2006). These climate changes over time were reconstructed through integrated analyses of historical documents, and the data has the advantages of high resolution, accurate ages and spatial locations.

Figure 9 shows that Ca concentrations were moderately positively correlated with temperature in LIA-2, but the Al concentrations were not clearly correlated with any of the climate factors we considered in LIA-2. These indicate that weathering status in LIA-2 may be out of the natural state.

The significant increase in population in LIA-2 (Figure 9E) led to a greater need for farmlands. Indeed, historical documents show that the total cultivated area in China increased markedly during LIA-2 (Ge et al., 2008). The development of new farmlands in LIA-2 had two major forms: first, new high yields crops suitable for cultivation in mountainous areas (including potatoes and maize) were generally popularized in China, and large areas of mountainous forests were reclaimed to farmlands (Ge et al., 2003a, Ge et al., 2008); second, immigration to border areas (including Inner Mongolia, an upwind area of Gonghai Lake in winter half year) spurred the development of farmlands (Jiang, 1993; Ge et al., 2011).

Agricultural practices can enhance both mechanical and chemical weathering. For example, ploughing increases the voids in soils in order to provide oxygen for the respiration of crop roots, this process causes soils to be more easily transported by wind or runoff, thus contributing to mechanical weathering. Deforestation can increase the exposure of soils to wind or runoff, these can also lead to increases in mechanical weathering. Therefore, we propose that changes in land usage owing to agricultural practices that accompanied with population growth in LIA-2 could exacerbate mechanical weathering, and that can explain the increase in Al concentrations in the Gonghai Lake sediments during this period. In terms of chemical weathering, humic materials are commonly used to fertilize soils, and those additions will increase soil acidity and promote the dissolution of Ca (Schlesinger and Durham, 2016). Moreover, chemical weathering can also be enhanced by agricultural irrigation. In light of these above, it can be inferred that the intensified agricultural activities could enhance both mechanical weathering and chemical weathering during LIA-2, which contradicted to the trade-off between them in LIA-1 or natural state (Chen et al., 1997).

The Al concentrations in LIA-2 were significantly lower than those in LIA-1, but they were about the same as those in the MWP (Figure 9C). As the climate in the LIA was cold, mechanical weathering should be strong and Al concentrations high. However, chemical weathering that resulted from the relatively developed agricultural activities in LIA-2 might increase the inputs of Ca and other chemical weathered materials to the lake, thereby reducing the proportion of the mechanically weathered Al input. Moreover, the input of other mechanically weathered major elements, Si, Fe, K, were also

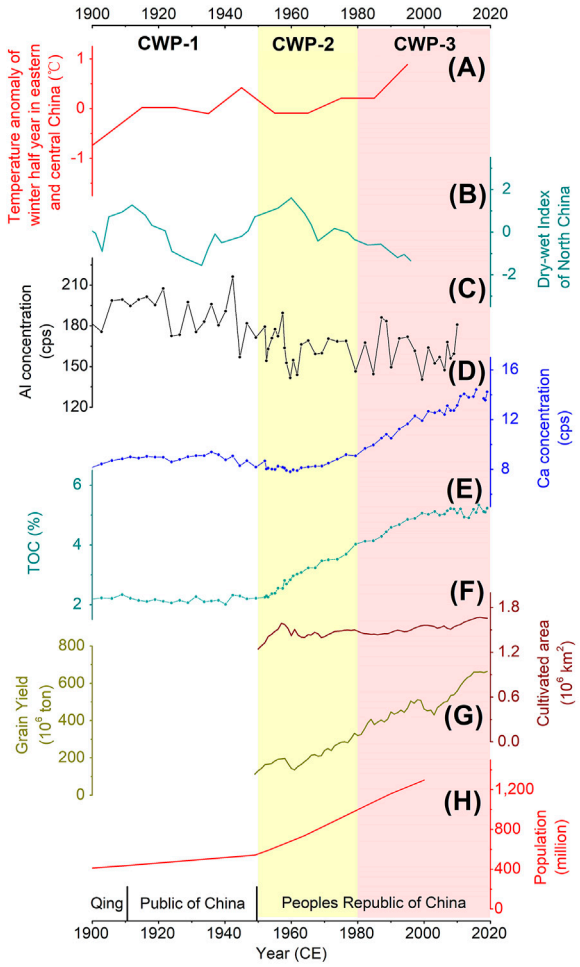

FIGURE 10
(A) Temperature anomaly for the winter half year in eastern and central China (Ge et al., 2003b), **(B)** dry-wet index in North China (Zheng et al., 2006), **(C,D)** Al, Ca concentrations, **(E)** total organic carbon (TOC) contents, and **(H)** population of China (Cao and Ge, 2005) in the Current Warming Period (CWP); **(F)** cultivated area and **(G)** grain yield in China after 1950 CE (Official website of the National Bureau of Statistics, n. d.). The yellow shadowed area indicates CWP-2, and the pink shadowed area indicates CWP-3.

reduced (Figures 7A–E), as Al, Si, Fe, K and other mechanically weathered materials account for most the mass of Gonghai Lake sediments (Shen et al., 2010), it is deduced that the total amount of material input to Gonghai Lake became less. This may be the reason that sedimentation rate in LIA-2 was relatively low (Figure 6B). More specifically, potatoes were planted in relatively cold areas around Gonghai Lake in LIA-2 (Ge et al., 2003a), and the associated agricultural development likely affected the inputs of Al and Ca from weathering. From the above, it can be inferred that human activities caused significant changes on weathered material inputs to Gonghai Lake in LIA-2.

6.6 Changes in Al and Ca concentrations in the Current Warming Period (post-1900 CE)

Human activities got more intensive during modern times. To see the trends for the time-series plots of the selected indicators in this period more distinctly, the data for the CWP was plotted separately in Figure 10. Based on the trends of the time-series plots of Al and Ca concentrations during this period, we divided the CWP into three stages: 1900–1950 CE (CWP-1), 1950–1980 CE (CWP-2), and post-1980 CE (CWP-3), which are discussed in sequence below.

6.6.1 CWP-1: 1900–1950 CE

During this period, Al and Ca concentrations showed very small changes despite the warmer and drier climate (Figures 10A–D). This provides another perspective on potential impacts of human activities on the elemental weathering indicators.

In CWP-1, the population of China increased from ~400 million to ~600 million (Figure 10H), and human activities increased concomitantly, but the cultivated area of China did not increase much during this period (Figure 10F, Ge and Dai, 2005). From this it can be inferred that agricultural activities were not likely to significantly affect mechanical weathering, and this may be the reason that Al concentrations did not change significantly in CWP-1.

On the other hand, it is expected that Ca concentrations increased owing to warmer climate and enhanced chemical weathering by agricultural activities, but the climate was drier (Figure 10B), and that might offset the effects of temperature on chemical weathering and thus Ca concentrations, resulting in relatively stable Ca concentrations during this stage.

Besides, wars and unstable political situation during this stage were adverse to socio-economic development, which may offset the impact of the increased population on weathering and thus Al and Ca concentrations.

6.6.2 CWP-2: 1950–1980 CE

In this stage, Al concentrations were significantly lower than those in CWP-1, while Ca concentrations in the earlier part were relatively stable but then increased moderately in the later part. The increase in Ca concentrations of the above may be related to the warmer climate in the 1960s–1970s, but in terms of the otherwise of the above, there were no apparent correlations to climate change (Figures 10A–D, yellow shadow area). During this period, the population of China increased from ~600 to ~1,000 million, ~70% growth rate (Figure 10H), and human activities increased accordingly, but there were not significant effects of population growth (i.e., enhanced human activities) on Al or Ca concentrations.

With the increase in population, there was a corresponding increase in grain output (Figure 10G), however, the area of cultivated land in China was almost unchanged during this

period (Figure 10F). Therefore, the impact of reclamation on mechanical weathering would not be substantive. On the other hand, it can be inferred that the yield per unit area rose with the increased total grain yield, and thus the organic matters content per unit area should also increase. This could increase exogenous organic matter input to Gonghai Lake. During this stage, the climate had not changed significantly, which had not notably impacted to the lake production; chemical fertilizer was in low level popularization owing to the low level of industrialization, so the eutrophication level of Gonghai Lake was not high. Therefore, it can be inferred that the increase in autochthonous source of organic matters was limited. In sum of the above factors, the input of organic matters to Gonghai Lake sediments increased during CWP-2 (indicated by total organic carbon contents, Figure 10E), while the relative proportion of inorganic matters, including Al, decreased.

For Ca, the increase in yield per unit area corresponded with an enhancement in agricultural activities, which increased chemical weathering and Ca deposition. However, increases in organic matters deposition to sediments would tend to reduce the proportion of inorganic matters in the sediments, including Ca. The combined effects of these two offsetting factors are a likely reason that Ca increased slightly only in the later part of CWP-2.

6.6.3 CWP-3: post-1980 CE

The significant increase in Ca in CWP-3 resulted from many factors. First, both the effects of remarkable agricultural development and rapid climate warming (Figure 10) aggravated chemical weathering and the migration of Ca. Second, Ca in the lake water was apt to be deposited for more intensive evaporation owing to the warmer and drier climate. Moreover, the productivity of the lake increased because much more reactive nitrogen was deposited (Cui et al., 2013); in this process, more CO_2 and HCO_3^- in the lake water were consumed, the pH value of the lake water increased, and thus more Ca was deposited (Shen et al., 2010).

Anthropogenic effects on the weathering of Al during this stage had both positive and negative effects as follows. After 1980 CE, industrial, mining, and urban land use increased mechanical weathering, and thus led to increases in Al fluxes to the lake. Although grain yield increased sharply, the cultivated area did not increase greatly (Figures 10F,G), so there was not significant impact on Al, similar to the conditions in CWP-2. There were several other factors that may have reduce Al concentrations, including: 1) a policy in China implemented after 1980 CE aimed at converting farmlands to forest—the forest vegetation increased during this stage (Ge et al., 2008) and should decrease mechanical weathering and Al concentrations; 2) the TOC contents increased significantly in this stage, and thus the inorganic materials, including Al, in sediments would decrease proportionately. The effects of the positive and negative factors could offset each other, in consequence, Al concentrations did not change significantly during this period.

6.7 Human impacts on the correlations between Al and Ca concentrations after 1550 CE

One of the main conclusions from the above is that, after 1550 CE, human activities significantly influenced the mechanical and chemical weathering of soils, and those processes affected the concentrations of various elements in Gonghai Lake sediments. As the concentrations of these elements in the sediments changed owing to additional anthropic factors on the background of natural factors, the correlations between the elements might also change.

In Subsection 6.4–6.6, the discussion of anthropogenic influences on sediment Ca and Al concentrations was divided into five stages: MWP and LIA-1, LIA-2, CWP-1, CWP-2, CWP-3. To illustrate the impacts of human activities, the correlations between Al and Ca concentrations in the five stages are summarized in Figure 11.

From 1000 to 1550 CE, the correlation between Al and Ca (Figure 11A) was same as that in the natural state (Chen et al., 1997; Shen et al., 2010), but after 1550 CE, the correlations changed (Figures 11B–E). This change support that human activities significantly influenced the weathering of soils around Gonghai Lake since 1550 CE mentioned in subsection 6.5 and 6.6.

The period of 1900–1950 CE is CWP-1, but the correlation between Al and Ca concentrations in this period is the same as that in LIA-2 (Figures 11B,C) even though LIA-2 and CWP-1 belong to different climate stages on centennial scale. In consideration of the change in correlation of Al and Ca concentrations after 1550 CE owing to human activities mentioned above, this supports that climate was not a major influence on weathering during LIA-2 and CWP-1 (i.e., 1550–1950 CE).

The AWG proposed ca. 1950 CE as the onset of the Anthropocene. The Al and Ca concentrations in Gonghai Lake sediments were uncorrelated after 1950 CE, which is different from those anti-correlated from 1550 to 1950 CE (Figures 11B–E). This suggests that human activities in the Anthropocene may have changed the weathering processes around Gonghai Lake.

6.8 Historical events recorded by Al and Ca concentration time-series plots

On decadal scale, it can be observed that Al and Ca concentration time-series plots recorded three historical events

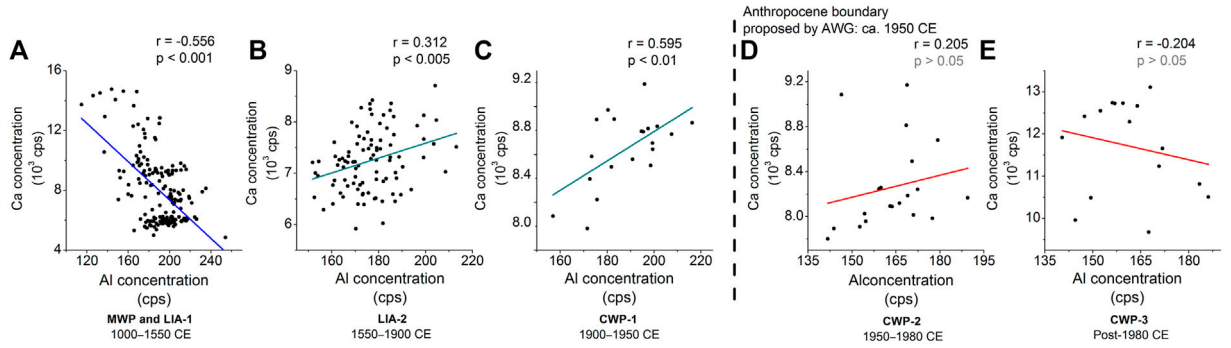

FIGURE 11
The Pearson correlation coefficient r and significance level *p*-value between Al and Ca concentrations in **(A)** the Medieval Warming Period (MWP) and Little Ice Age-1 (LIA-1), **(B)** Little Ice Age-2 (LIA-2), and **(C–E)** three stages of the Current Warming Period (CWP-1, CWP-2, CWP-3) of Gonghai Lake. The dashed line indicates the onset of the Anthropocene proposed by the AWG.

after 1550 CE, one border reclamation project and two catastrophic decreases in population.

6.8.1 Border reclamation project in the 16th century

The LIA was separated into LIA-1 and LIA-2 based on significant difference of element concentrations and the changes in the correlation between Al and Ca concentrations before and after 1550 CE. There was no sharp climate change around 1550 CE. Therefore, it raises the question as to why there was a peak in Al concentrations plot followed by a sudden decrease around that time (Figure 9 cyan column), and why there were significant increase in Ca concentrations.

Under this condition, we decided to investigate the possibility that human activities affected weathering processes during this period. In the 16th century, China's population increased significantly (Figure 9E), the climate turned warm and humid (Figures 9A,B), and thus the agro-pastoral ecotone moved northward (Ge et al., 2011). To make use of the arable land in border areas and alleviate the increasing population pressure on the mainland, the government implemented a border reclamation project and an immigration policy (Ge et al., 2011). Reclamation of lands for planting would promote mechanical weathering through the removal of native vegetation and disturbances to the soils (Ge et al., 2011), and in this particular case, increased quantities of mechanically weathered materials may have been transported as dust particles to the downwind areas including Gonghai Lake.

Dust storms in China were often referred to as "soil rain" in historical documents. Zhang (1982) reviewed records of soil rain events in North China in historical times, and found that soil rain events were less frequent during warm and humid periods. But the "soil rain" in the 16th century did not match this relationship, that is, the climate was warm and humid during that period (Ge et al., 2011), but there was a relatively high frequency of soil rain events. In light of the peak in the Al concentrations time-series plot in the same period, we propose that the border reclamation project was a possible cause for to the increased soil rain events. The border reclamation project raised the dust, which was transported and deposited in Gonghai Lake, thereby increasing the inorganic inputs and leading to the peak in the Al and Ca concentrations time-series plot.

After the initial reclamation, the land was planted with crops. The mechanical weathering from farmland management was less intensive than that from the initial reclaiming, and thus the Al and Ca input decreased, resulting in the decrease in Al and Ca concentrations. On the other hand, the agricultural activities also enhanced chemical weathering. Therefore, the Ca concentrations decreased only in the initial period, but increased afterwards.

6.8.2 Catastrophic decreases in population

In the above text, we discussed the possibility that weathering state around Gonghai Lake was significantly influenced by human activities after 1550 CE. In addition to the effects of the intensified human activities, dramatic decreases in population and thus human activities were also recorded. Indeed, there were two population crashes after 1550 CE: one was at the end of the Ming Dynasty from 1630s to 1640s, and the other was in the late Qing Dynasty from 1850s to 1870s. These two catastrophic events were resulted from war, drought, and famine (Ge et al., 2011).

From 1850s to 1870s in the late Qing Dynasty, Al and Ca concentrations decreased significantly (Figure 9, gray column II), possibly in response to a decrease in population (Cao and Ge, 2005). Reductions in agricultural activities would lead to a weakening of chemical and mechanical weathering, and that in turn would reduce the inputs of Al and Ca to Gonghai Lake. On the other hand, a decrease in Ca concentrations preceded that of Al, possibly in response to a cooler climate and a weakening of chemical weathering, the colder climate in the 1870s was also a

possible reason for the decrease of Ca concentrations. However, these were regardless of Al concentrations decrease, which should be resulted from the weakening human activities.

In the catastrophic event during 1630s–1640s at the end of Ming Dynasty, The Al concentrations decreased significantly with the markedly drier climate, this is regardless of the climate change but may be due to the weakening human activities and the sequential restoration of natural vegetation. However, Ca concentrations did not decrease significantly during this period. There are two factors could influence Ca concentrations. One is that the climate became drier and chemical weathering weakened and thus decreased Ca concentrations, the other is the restoration of vegetation intensified chemical weathering, leading to an increase in Ca concentration. The above two factors could offset each other, so the changes in Ca concentrations were not obvious. In addition, from 1610s to 1620s, the Ca decrease might be a response to the climate drying (Figure 9), which indicates that climate change still had a considerable impact on Ca inputs to the lake during this period. In summary, the changes in Ca concentrations caused by human activities at the end of Ming Dynasty were not so pronounced as those in the late Qing Dynasty. This may be because the population of China was ~200 million in the late Ming Dynasty, but reached ~440 million before the outbreak of Taiping Heavenly Kingdom War in the late Qing Dynasty (1851 CE) (Figure 9E). In other words, the environmental responses to human activity change captured in the lake sediments evidently varied with the magnitude of the anthropogenic perturbations on the natural systems.

7 Conclusion

The analysis of data for Al and Ca concentrations in lake sediments since 1000 CE in combination with the history of China has led us to the following conclusions.

Changes in Al, Ca concentrations and changes in correlations between them show that weathering processes around Gonghai Lake changed after 1550 CE and moved it from the natural state. This can be attributed to the agricultural activities that enhanced both mechanical and chemical weathering.

1900 CE is considered as the boundary between the LIA and the CWP, however, the correlations between Ca and Al concentrations did not change in the two periods before and after this time boundary (1550–1900 CE and 1900–1950 CE). Referring to that the correlation changed around 1550 CE owing to human activities, it is inferred that the weathering state did not change significantly around 1900 CE, and more importantly, climate change in this period was not a decisive influence on weathering.

Changes in the correlations between Al and Ca concentrations at 1950 CE indicate that weathering processes changed after 1950 CE, the stage of the Anthropocene that was proposed by the AWG. More detailed analyses show that the weathering history recorded in Gonghai Lake sediments during the Anthropocene proposed by the AWG can be divided into two stages: 1950–1980 CE and post-1980 CE. The socio-economic development during these two stages affected land use and hence weathering.

Weathering processes recorded by Gonghai Lake sediments after 1550 CE were shown to coincide with three historical events, these include the border reclamation project in northern border areas of China in the 16th century, the catastrophic crashes in population from 1630s to 1640s at the end of Ming Dynasty and from 1850s to 1870s in the late Qing Dynasty. The elemental records of chemical and mechanical weathering preserved in the lake sediments provide information on the impacts of human activities on the Earth system that may prove useful references for resource and environmental management.

Data availability statement

The data obtained by the methods of this paper are openly available in East Asian Paleoenvironmental Science Database, (http://paleodata.ieecas.cn/index.aspx), doi: 10.12262/IEECAS.EAPSD2022002.

Author contributions

HJ, YH: Conceptualization; HJ: Experiment, data analysis, original draft writing; YH YT, and RA: Writing-reviewing and editing; YH: Funding acquisition; HF and BL: Experiment.

Funding

This study was supported by the National Natural Science Foundation of China (41991250) and the Strategic Priority Research Program of Chinese Academy of Sciences (XDB40000000).

Acknowledgments

We acknowledge the National Observation and Research Station of Regional Ecological Environment Change and Comprehensive Management in the Guanzhong Plain, Shaanxi.

Conflict of interest

The authors declare that the research was conducted in the absence of any commercial or financial relationships that could be construed as a potential conflict of interest.

Publisher's note

References

Cao, S., and Ge, J. (2005). *History of Chinese population*, Vol. V. Shanghai: Fudan University Press, 704–832. (in Chinese).

Chen, F., Chen, S., Zhang, X., Chen, J., Wang, X., Gowan, E. J., et al. (2020). Asian dust-storm activity dominated by Chinese dynasty changes since 2000 BP. *Nat. Commun.* 11, 992. doi:10.1038/s41467-020-14765-4

Chen, F., Xu, Q., Chen, J., Birks, H. J. B., Liu, J., Zhang, S., et al. (2015). East Asian summer monsoon precipitation variability since the last deglaciation. *Sci. Rep.* 5, 11186. doi:10.1038/srep11186

Chen, J., Ji, J., Qiu, G., Lu, H., and Zhu, H. B. (1997). Geochemical study on chemical weathering degree of loess in Luochuan County, Shaanxi Province. *Sci. China (Series D)* 27 (6), 531–536. (In Chinese). doi:10.3321/j.issn:1006–9267.1997.06.004

Chen, S., Liu, J., Xie, C., Chen, J., Wang, H., Wang, Z., et al. (2018). Evolution of integrated lake status since the last deglaciation: A high-resolution sedimentary record from lake Gonghai, Shanxi, China. *Palaeogeogr. Palaeoclimatol. Palaeoecol.* 496, 175–182. doi:10.1016/j.palaeo.2018.01.035

Chen, S., Wang, X., Chen, J., Liu, J., Wang, Z., Qiang, M., et al. (2017). The modern processes of atmospheric dust record by sediments from Gonghai Lake, Shanxi, China. *J. Desert Res.* 37 (2), 228–236. (in Chinese with English abstract). doi:10.7522/j.issn.1000-694X.2016.00096

Cheng, B., Liu, J., Chen, S., Zhang, Z., Shen, Z., Yan, X., et al. (2020). Impact of abrupt late Holocene monsoon climate change on the status of an alpine lake in North China. *J. Geophys. Res. Atmos.* 125, e2019JD031877. doi:10.1029/2019JD031877

Crutzen, P. J. (2002). Geology of mankind. *Nature* 415, 686723. doi:10.1038/415023a

Cui, S., Shi, Y., Groffman, P. M., Schlesinger, W. H., and Zhu, Y. (2013). Centennial-scale analysis of the creation and fate of reactive nitrogen in China (1910–2010). *Proc. Natl. Acad. Sci. U. S. A.* 110 (6), 2052–2057. doi:10.1073/pnas.1221638110

Davies, S. J., Lamb, H. F., and Roberts, S. J. (2015). Micro-XRF core scanning in palaeolimnology: recent developments. *Dev. Paleoenviron. Res.* 17, 189–226. doi:10.1007/978-94-017-9849-5_7

Ge, Q., and Dai, J. (2005). Analysis of agricultural and forestry land use change and its driving factors in China in early and middle 20th century. *Sci. China Ser. D Earth Sci.* 35 (1), 54–63. (in Chinese). doi:10.3321/j.issn:1006-9267.2005.01.006

Ge, Q., Dai, J., and He, F. (2008). *Land use change and terrestrial carbon budgets in China during the last 300 years*. Beijing: Science Press, 32–231. (in Chinese).

Ge, Q., Dai, J., He, F., Zheng, J., Man, Z., and Zhao, Y. (2003a). Analysis on quantitative changes and driving factors of cultivated land resources in some provinces and regions of China in the past 300 years. *Prog. Nat. Sci.* 13 (8), 825–833. (in Chinese). doi:10.3321/j.issn:1002-008X.2003.08.008

Ge, Q., Zhang, P., Zheng, J., Liu, H., He, F., Fu, H., et al. (2011). *Climate change in China's past dynasties*. Beijing: Science Press, 430–550. (in Chinese).

Ge, Q., Zheng, J., Fang, X., Man, Z., Zhang, X., Zhang, P., et al. (2003b). Winter half-year temperature reconstruction for the middle and lower reaches of the Yellow River and Yangtze River, China, during the past 2000 years. *Holocene* 13 (6), 933–940. doi:10.1191/0959683603hl680rr

Han, Y. M., Cao, J. J., Kenna, T. C., Yan, B., Jin, Z. D., Wu, F., et al. (2011). Distribution and ecotoxicological significance of trace element contamination in a 150 yr record of sediments in Lake Chaohu, Eastern China. *J. Environ. Monit.* 13, 743–752. doi:10.1039/c0em00551g

Han, Y. M., Wei, C., Huang, R.-J., Bandowe, B. A. M., Ho, S. S. H., Cao, J. J., et al. (2016). Reconstruction of atmospheric soot history in inland regions from lake sediments over the past 150 years. *Sci. Rep.* 6, 19151. doi:10.1038/srep19151

Huang, J., Lu, S. N., Chue, P. Y., Lee, C. M., Yu, M. L., Chuang, W. L., et al. (2001). Hepatitis C virus infection among teenagers in an endemic township in taiwan: epidemiological and clinical follow-up studies. *Epidemiol. Infect.* 35 (4), 485–492. (In Chinese with English abstract). doi:10.1017/s0950268801006148

Jiang, T. (1993). *Population history of modern China*. Hangzhou: Zhejiang People's Publishing House, 199–213. (in Chinese).

Lewis, S. L., and Maslin, M. A. (2015). Defining the Anthropocene. *Nature* 519, 171–180. doi:10.1038/nature14258

Liu, E., Xue, B., Yang, X., Wu, Y., and Xia, W. (2009). 137Cs and 210Pb chronology for modern lake sediment: A case study of chaohu lake and taibai lake. *Mar. Geol. Quat. Geol.* 29 (6), 89–94. (in Chinese with English abstract). doi:10.3724/SP.J.1140.2009.06089

Liu, J., Chen, F., Chen, J., Xia, D., Xu, Q., Wang, Z., et al. (2011). Humid medieval Warm Period recorded by magnetic characteristics of sediments from Gonghai Lake, Shanxi, north China. *Chin. Sci. Bull.* 56 (23), 2464–2474. doi:10.1007/s11434-011-4592-y

Liu, J., Chen, J., Selvaraj, K., Xu, Q., Wang, Z., and Chen, F. (2014). Chemical weathering over the last 1200 years recorded in the sediments of Gonghai Lake, lvliang mountains, north China: a high-resolution proxy of past climate. *Boreas* 43 (4), 914–923. doi:10.1111/bor.12072

Liu, Y., Chen, G., Meyer-Jacob, C., Huang, L., Liu, X., Huang, G., et al. (2021). Land–use and climate controls on aquatic carbon cycling and phototrophs in karst lakes of southwest China. *Sci. Total Environ.* 751, 141738. doi:10.1016/j.scitotenv.2020.141738

Liu, Y., Song, H. M., An, Z., Sun, C., Trouet, V., Cai, Q., et al. (2020). Recent anthropogenic curtailing of Yellow River runoff and sediment load is unprecedented over the past 500 y. *Proc. Natl. Acad. Sci. U. S. A.* 117 (31), 18251–18257. doi:10.1073/pnas.1922349117

Schlesinger, W. H., and Durham, E. S. (2016). *Biogeochemistry–an analysis of global change*. Beijing: Science Press, 77–82. (in Chinese).

Shen, J., Xue, B., Wu, J., Wu, Y., Liu, X., Yang, X., et al. (2010). *Lake sedimentation and environmental evolution*. Beijing: Science Press, 180–184. (in Chinese).

Shu, L. (2010). *Physical geology*. Beijing: Geological Publishing House, 70–71. (in Chinese).

Tan, Q. (1962). Why did the Yellow River have a long-term stable flow after the eastern han dynasty. *Acad. Mon.* 2, 23–35. in Chinese. doi:10.19862/j.cnki.xsyk.1962.02.005

Wan, D., Song, L., Yang, J., Jin, Z., Zhan, C., Mao, X., et al. (2016). Increasing heavy metals in the background atmosphere of central North China since the 1980s: Evidence from a 200-year lake sediment record. *Atmos. Environ.* 138, 183–190. doi:10.1016/j.atmosenv.2016.05.015

Wang, S. (2011). *The Holocene climate change*. Beijing: China Meteorological Press, 122–124. (in Chinese).

Wang, Y., Cheng, H., Edwards, R. L., He, Y., Kong, X., An, Z., et al. (2005). The Holocene asian monsoon: Links to solar changes and north atlantic climate. *Science* 308, 854–857. doi:10.1126/science.1106296

Waters, C. N., Zalasiewicz, J., Summerhayes, C., Barnosky, A. D., Poirier, C., Galuszka, A., et al. (2016). The Anthropocene is functionally and stratigraphically distinct from the Holocene. *Science* 351 (6269), aad2622–10. doi:10.1126/science.aad2622

Waters, C. N., Zalasiewicz, J., Summerhayes, C., Fairchild, I. J., Rose, N. L., Loader, N. J., et al. (2018). Global boundary stratotype section and point (GSSP) for the Anthropocene series: Where and how to look for potential candidates. *Earth-Science Rev.* 178, 379–429. doi:10.1016/j.earscirev.2017.12.016

Wu, D., Zhou, A., Liu, J., Chen, X., Wei, H., Sun, H., et al. (2015). Changing intensity of human activity over the last 2, 000 years recorded by the magnetic characteristics of sediments from Xingyun Lake, Yunnan, China. *J. Paleolimnol.* 53, 47–60. doi:10.1007/s10933-014-9806-2

Zhang, D. (1982). Analysis of "soil raining" phenomenon in historical period. *Chin. Sci. Bull.* 5, 294–297. (in Chinese). doi:10.1360/csb1982-27-5-294

Zhang, P., Cheng, H., Edwards, R. L., Chen, F., Wang, Y., Yang, X., et al. (2008). A test of climate, sun, and culture relationships from an 1810-year Chinese cave record. *Science* 322, 940–942. doi:10.1126/science.1163965

Zheng, J., Wang, W.-C., Ge, Q., Man, Z., and Zhang, P. (2006). Precipitation variability and extreme events in eastern China during the past 1500 Years. *Terr. Atmos. Ocean. Sci.* 17 (3), 579–592. doi:10.3319/tao.2006.17.3.579(a)

Zong, Y., Yu, F., Huang, G., Lloyd, J. M., and Yim, W.-S. (2010). Sedimentary evidence of late Holocene human activity in the pearl river delta, China. *Earth Surf. Process. Landf.* 35, 1095–1102. doi:10.1002/esp.1970